OPEN ACCESS

Middle East Research Journal of Biological Sciences
ISSN 2789-7710 (Print & ISSN 2958-2091 (Online)
Frequency: Bi-Monthly
DOI: 10.36348/merjbs.2024.v04i04.002

KUWAIT SCHOLARS PUBLISHER
Website: http://www.kspublisher.com/
Email: office@kspublisher.com

Use Remote Sensing, GIS and Regression Analysis in Monitoring Water Quality of Al-Gharraf River Southern of Iraq

Wisam Thamer Al-Mayah[1*], Wisam Basim Al-Tmemy[2]
[1]Department of Basic Science, College of Dentistry, University of Wasit, Iraq
[2]Department of Medical Laboratory Technologies, AL KUT University College, Iraq

Abstract: Water quality of Al-Gharraf River, the largest branch of Tigris River south of Iraq, was evaluated using the first seven bands Landsat-8 OLI images acquired on 19 January 2017, 24 April 2017, 14 July 2017 and 20 November 2017, at twenty-one measured stations along the Al-Gharraf River. The multiple linear regression models were developed to found the relationship between the water quality parameters (CHL-a, DOM, NTU, TSS, and TDS), as independent variables and Landsat 8 OLI spectral data as dependent variables. Among these models, the most appropriate models with highest R^2 value were selected. Once the developed models applied in order to have maps with a variation of colors can be used to estimate the water quality classification at any point along the river.

Keywords: Remote sensing, GIS, regression model, Al-Gharraf River, Water quality.

RESEARCH PAPER

***Corresponding Author:**
Wisam Thamer Al-Mayah
Department of Basic Science, College of Dentistry, University of Wasit, Iraq

How to cite this paper:
Wisam Thamer Al-Mayah & Wisam Basim Al-Tmemy (2024). Use Remote Sensing, GIS and Regression Analysis in Monitoring Water Quality of Al-Gharraf River Southern of Iraq. *Middle East Res J Biological Sci*, *4*(4): 96-112.

Article History:
| Submit: 29.05.2024 |
| Accepted: 01.07.2024 |
| Published: 08.07.2024 |

INTRODUCTION

In Iraq the application of remote sensing (RS) through water quality parameteres monitoring is still new. Generally the purpose of the monitoring of water quality parameteres in Iraq using remote sensing technique are because of the limit of the field cost, to improve the information contents, to produce the digital maps, and to monitoring the large scale monitoring of water quality that will offer the significance source of information.

Remote sensing techniques with GIS are useful tool due to their ability cover large areas with high spatial resolution, as well as it have spatial and temporal view of surface water quality parameters and more effectively and efficiently monitor the waterbodies, and quantify water quality problems (Gholizadeh, *et al.*, 2016). The Al-Gharraf River is of essential importance for domestic, agricultural and industrial uses and its water masses are essential to satisfy requirements of Wasit and Dhi-Qar provinces. However, no published work was found to assess water quality of the Al-Gharraf River by using Al-Gharraf River by using remote sensing techniques and GIS. They study aimed is to predict the spatial distribution of water quality variables using satellite images during four seasons. remote sensing techniques and GIS. The study aimed is to predict the spatial distribution of water quality variables using satellite images during four seasons.

MATERIALS AND METHODS

Study Area

The Gharraf River is one of two branches of the Tigris River at Kutt City, 225 km south of Baghdad City. After branching from the Tigris, the Gharaff flows southeast toward Dhi- Qar governorate. The river is 230 km in length with a variable depth of 36 m at its branching point from the Tigris to 15 m at its junction with the Euphrates River at the marsh area near Naserya City. The coordinates of Gharraf River are lies between the north latitude (32° 27′ to 31° 2′ N) and east longitude (45° 45′ to 46° 4′ E). Its basin populated by more than 2 million people using about 432000 m³/year of refined water and passing through an agricultural area of about 215019 h in the south west of Iraq within the sediment plain (MOA and I, 1991). Figure (1): showed the map and the sampling stations of the study area.

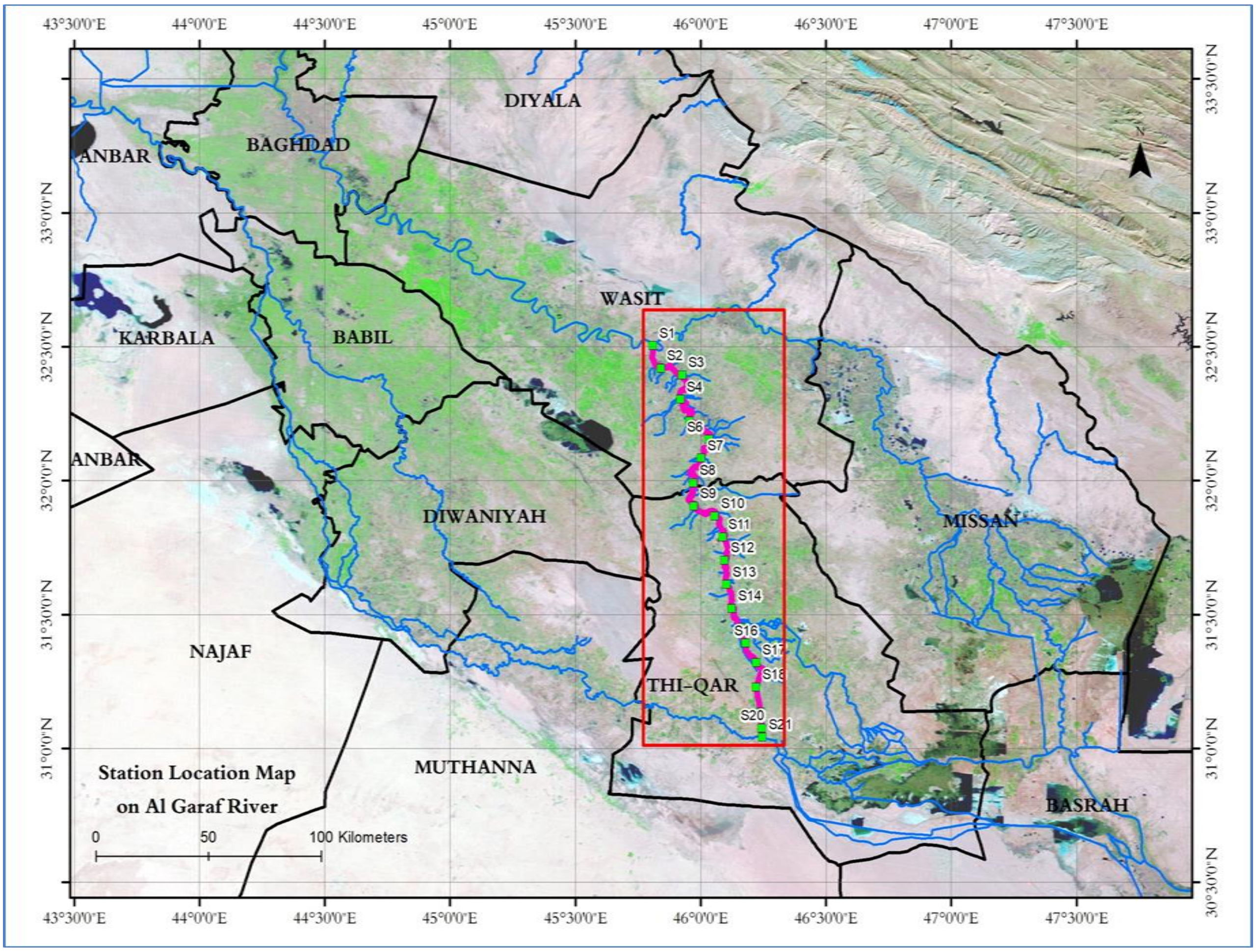

Fig. 1: Map of Al-Gharraf River showing the stations of the case study

Field Sampling and Analytical Procedures.

The collected water samples from the 21 point stations within Al-Gharraf river, during 12 months from January 2017 to December 2017, were preserved and analyzed according to American Public Health Association (APHA, 2015).

Image Processing

The remote sensed data image which used in this study include four Landsat-8 OLI images (path: 167 and row: 38) acquired on 19 January 2017, 24 April 2017, 14 July 2017 and 20 November 2017 which was coincident with the timing of fieldwork data collection as shown in Figure (2, 3, 4, and 5) respectively. The images were downloaded from the United State Geological Survey (USGS,2017. http://glovis.usgs.gov/).

For the spatial interpolation of the geometric correction, the image's original digital numbers (DNs) were preserved by subsequently using a Bilinear resampling method. After geometric correction, the images were atmospherically corrected. The atmosphere may potentially affect image by absorbing, scattering, and refracting light (Fan, 2014). histi

Atmospheric correction is carried out to minimize these atmospheric effects and convert digital numbers (DNs) to at-sensor reflectance values (Luyan *et al.*, 2015). ENVI 5.1 software has been used for geospatial analysis and spectral image processing of Landsat 8 OLI data imagery. It provides a tool called radiometric calibration undertakes this process for many data products that are distributed with calibration gain and offset values in the metadata (Abdullah, 2015).

Finally, empirical or analytical relationships between spectral properties and water quality parameters are established according to following equation:

$$Y = A + BX \; or \; Y = AB^X$$

Where: Y= is the remote sensing measurement (i.e., radiance, reflectance, energy), X= is the water quality parameter of interest (i.e., TSS, TDS, Chlorophyll), A and B are empirically derived factors.

In empirical approaches statistical relationships are determined between measured spectral/thermal properties and measured water quality parameters. Often information about the spectral/optical characteristic of the water quality parameter is used to aid in the selection of best wavelength(s) or best model in this empirical approach (Schmugge *et al.*, 2002).

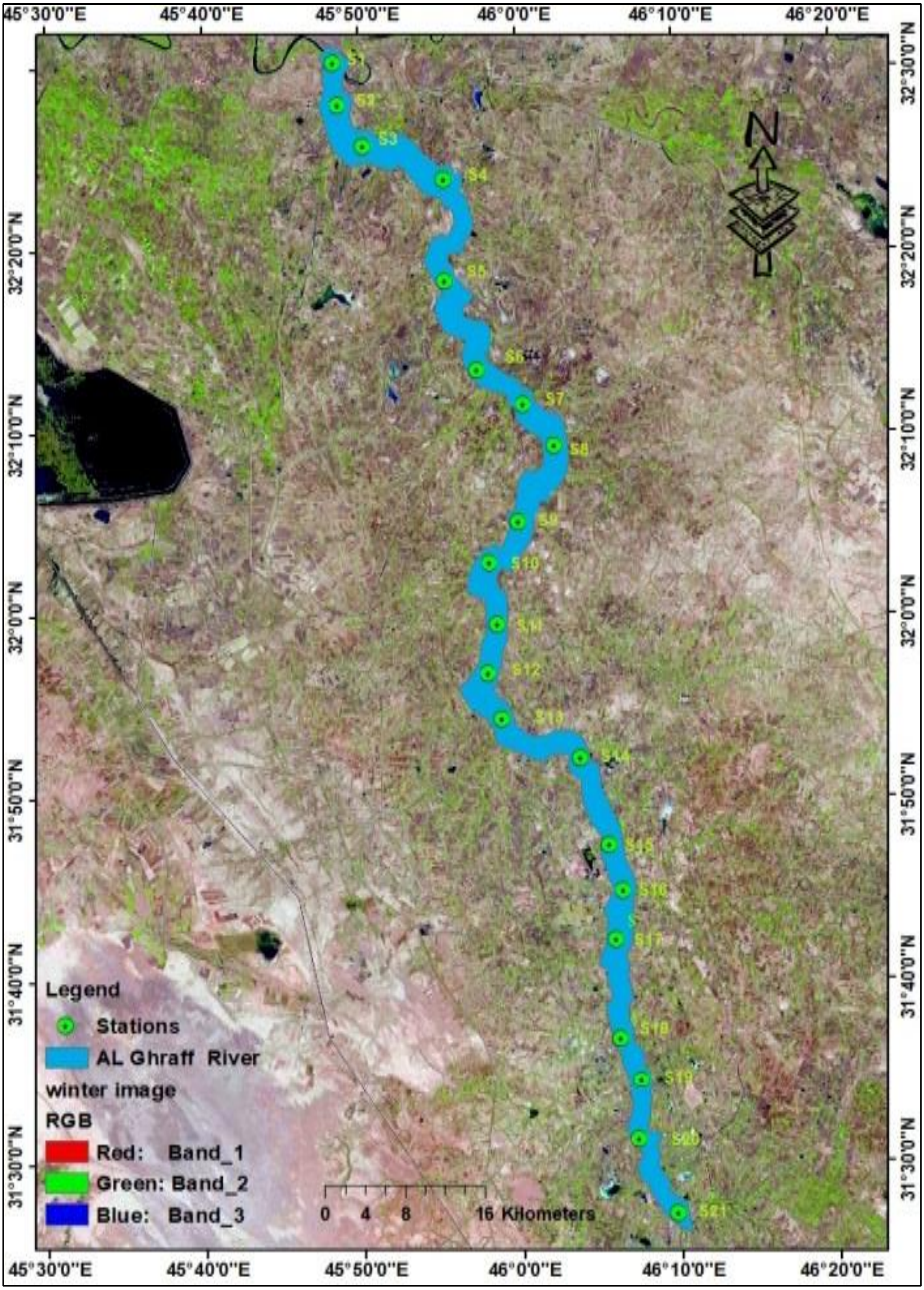

Fig. 2: Displays Landsat 8 OLI image on 20 February 2017 after processing

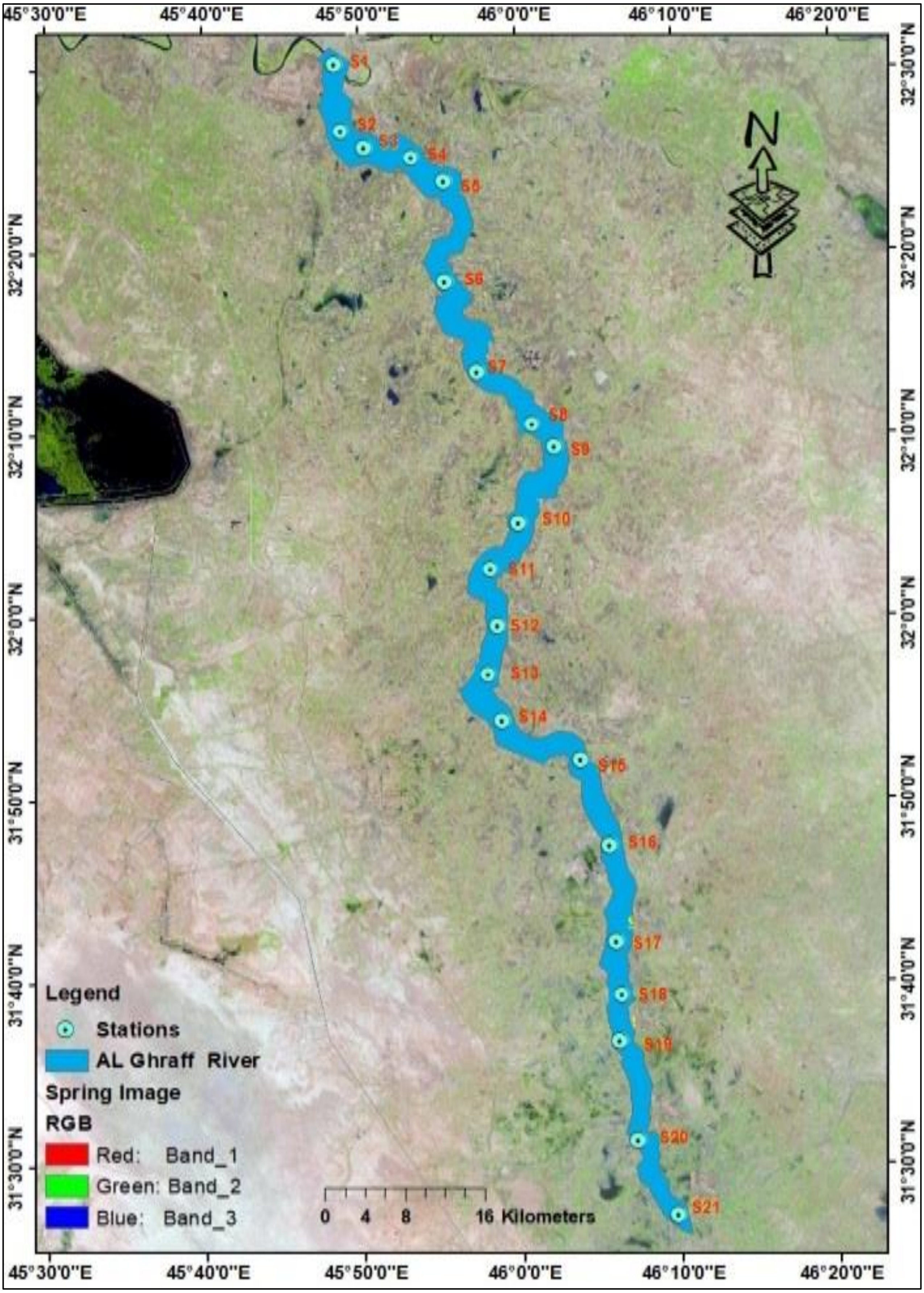

Fig. 3: Displays Landsat 8 OLI image on 25 April 2017 after processing

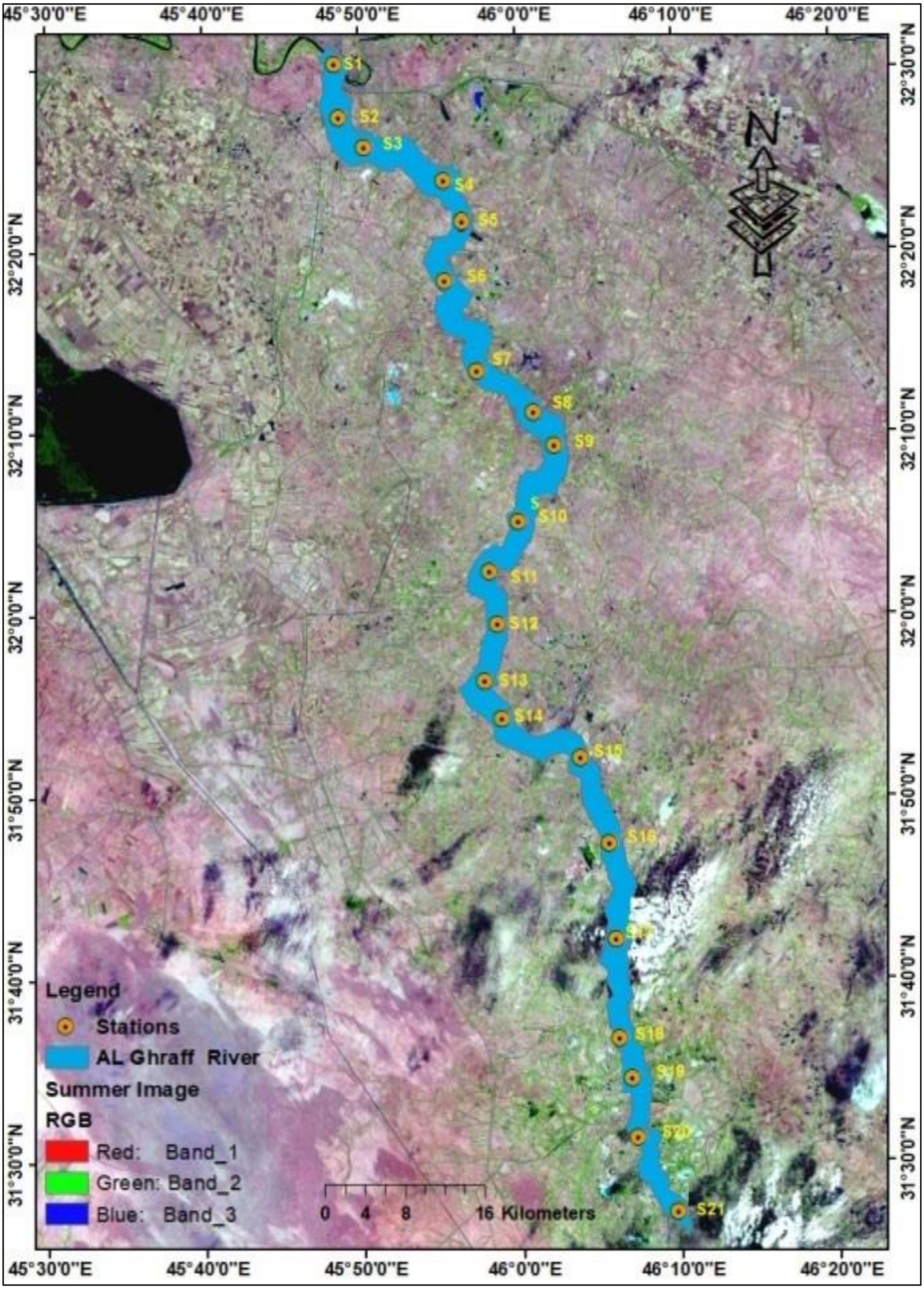

Fig. 4: Displays Landsat 8 OLI image on 14 July 2017 after processing

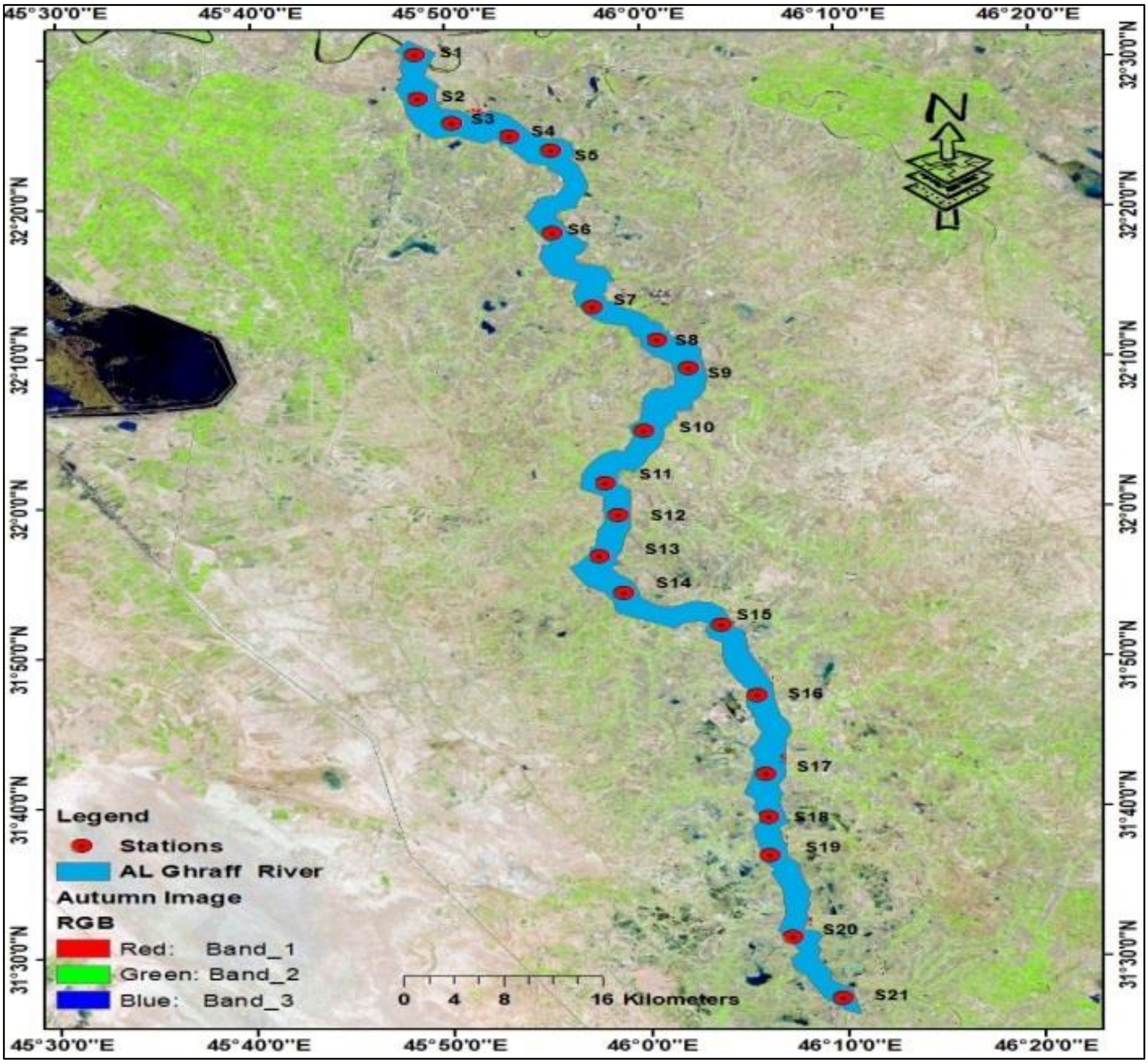

Fig. 5: Displays Landsat 8 OLI image on 5 November 2017 after processing

RESULTS AND DISCUSSION

Tabular (1, 2 and 3) illustrate mean, standard deviation (SD), correlation coefficient (r) and values of the reflectance in bands 1–7 at twenty-one stations along of the Al-Gharraf River respectively. It is noticed that there is an increase in the annual mean value of band 3 at Al-Gharraf River station because of the increasing of chlorophyll in the water. Besides, the reason for increasing the bands 2, 4 and 5 at river station was increasing the turbidity and dissolved organic matter in the water.

Table 1: Mean and standard deviation of different bands from the Al-Gharraf stations

Bands \ Statistic value	Mean	Standard deviation
B1	0.076	0.0318
B2	0.081	0.0323
B3	0.123	0.0338
B4	0.119	0.050
B5	0.091	0.0797
B6	0.077	0.0691
B7	0.062	0.0528

Table 2: Correlation coefficients for the seven bands in Iraq Landsat 8 OLI image at the Al-Gharraf stations

Correlation	Band1	Band2	Band3	Band4	Band5	Band6	Band7
Band 1	1.000	0.992**	0.956**	0.941**	0.911**	0.865**	0.877**
Band 2	0.992**	1.000	0.975**	0.954**	0.904**	0.889**	0.903**
Band 3	0.956**	0.975**	1.000	0.981**	0.905**	0.921**	0.927**
Band 4	0.941**	0.954**	0.981**	1.000	0.915**	0.893**	0.897**
Band 5	0.911**	0.904**	0.905**	0.915**	1.000	0.938**	0.933**
Band 6	0.865**	0.889**	0.921**	0.893**	0.938**	1.000	0.996**
Band 7	0.877**	0.903**	0.927**	0.897**	0.933**	0.996**	1.000

Table 3: Satellite image reflectance values in bands 1-7 at twenty-one stations

ID	Bands / Stations	Band1 0.43 - 0.45 (µm)	Band2 0.45 - 0.52 (µm)	Band3 0.53 - 0.59 (µm)	Band4 0.64 - 0.67 (µm)	Band5 0.76 - 0.90 (µm)	Band6 1.57 -1.65 (µm)	Band7 2.11-2.29 (µm)
S1	Ent. Kut	0.071	0.075	0.110	0.099	0.049	0.045	0.038
S2	End Kut	0.073	0.077	0.116	0.107	0.055	0.049	0.039
S3	Ent. Al-Muwaffaqiyah	0.068	0.072	0.111	0.103	0.059	0.054	0.043
S4	End Al-Muwaffaqiyah	0.070	0.074	0.115	0.108	0.067	0.055	0.045
S5	Ent. Al-Hayy	0.071	0.076	0.117	0.109	0.058	0.053	0.043
S6	Mid Al-Hayy	0.067	0.072	0.115	0.108	0.061	0.052	0.042
S7	End Al-Hayy	0.082	0.086	0.129	0.139	0.175	0.148	0.112
S8	Ent. Al-Fajr	0.076	0.079	0.120	0.114	0.086	0.074	0.058
S9	End Al-Fajr	0.073	0.077	0.118	0.113	0.078	0.066	0.050
S10	Ent. Qalat Sukar	0.093	0.098	0.131	0.129	0.097	0.068	0.062
S11	End Qalat Sukar	0.077	0.083	0.128	0.124	0.075	0.066	0.054
S12	Ent.Al-Rifai	0.085	0.096	0.142	0.139	0.114	0.139	0.114
S13	End Al-Rifai	0.079	0.085	0.129	0.124	0.083	0.068	0.053
S14	Ent. Al-Neser	0.081	0.086	0.131	0.133	0.119	0.095	0.076
S15	End Al-Neser	0.084	0.085	0.130	0.133	0.165	0.116	0.089
S16	Ent. Al-Shatrah	0.072	0.076	0.117	0.109	0.074	0.070	0.056
S17	Mid Al-Shatrah	0.083	0.086	0.131	0.129	0.120	0.090	0.071
S18	End Al-Shatrah	0.072	0.078	0.119	0.116	0.078	0.061	0.047
S19	Ent. Al-Gharraf	0.085	0.089	0.132	0.133	0.136	0.115	0.089
S20	Mid Al-Gharraf	0.073	0.077	0.121	0.117	0.088	0.071	0.057
S21	End Al-Gharraf	0.068	0.073	0.115	0.113	0.077	0.067	0.055

One other side, most of the studies prove that there are three important optical properties used for monitoring water quality such as concentration of the chlorophyll (CHL-a), total suspended matter (TSM) and color dissolved organic matter (DOM). In ocean, lake and river water, the major constituents are the CHL-a, TSM, DOM and the water itself causing absorption and scattering of light.

However, most chemicals and pathogens do not directly affect or change the spectral or thermal properties of surface waters so they can only be inferred indirectly from measurements of other water quality parameters affected by these chemicals (Lim and Choi, 2015).

Furthermore, the multiple linear regression models were developed to found the relationship between the water quality parameters (CHL-a, DOM, NTU, TSS, and TDS), as independent variables and Landsat 8 OLI spectral data as dependent variables. Among these models, the most appropriate models with highest R^2 value were selected. The R2 value for some water quality parameters models were decreased due to decreasing the reflectance of Landsat 8 OLI that captured during study period and seasonal changes of water quality parameters of Al-Gharraf River.

Also, the reduction of reflectance is due to the light penetration from water surface, intensity of incipient of light, angle of ray incidence and scattering and absorption light within the water. In the study area all the water quality parameters showed a wide variation in space and time along Al-Gharraf River. Temporal variations were due to seasonal influences mainly, the effect of rainfall.

Table 4 display the R^2 value and coefficients values of regression equations for each water quality parameter. As well as, correlation coefficient of seasonal the Landsat reflectance data and most important optical properties used for monitoring water quality as presented in Table 5.

Table 4: Landsat reflectance data correlation and water quality parameters during study period 2016-2017

Reflectance / Parameter	Winter (19 January, 2017)						
	Band1	**Band2**	**Band3**	**Band4**	**Band5**	**Band6**	**Band7**
CHL-a mg/l	-0.32 NS	0.85 **	0.33 NS	0.30 NS	0.26 NS	0.28 NS	0.27 NS
DOM mg/l	-0.29 NS	-0.25 NS	0.42 *	0.27 NS	0.19 NS	0.21 NS	0.21 NS
Turbidity NTU	-0.49 *	-0.37 *	0.31 NS	0.10 NS	0.03 NS	0.05 NS	0.05 NS
TSS mg/l	-0.33 NS	-0.21 NS	0.36 *	0.35 *	0.30 NS	0.32 NS	0.33 NS
TDS mg/l	-0.44 *	-0.31 NS	0.31 NS	0.13 NS	0.01 NS	0.04 NS	0.06 NS
Spring (24 April, 2017)							
CHL-a mg/l	0.28 NS	0.31 NS	0.72 **	0.71*	0.76 **	0.34 NS	0.31 NS
DOM mg/l	0.23 NS	0.40 *	0.33 NS	0.48 *	0.35 *	0.29 NS	0.33 NS
Turbidity NTU	0.30 NS	0.28 NS	0.34 NS	0.36 *	0.40 *	0.35 *	0.31 NS
TSS mg/l	0.33 NS	0.30 NS	0.34 NS	0.39 *	0.43 *	0.40 *	0.32 NS
TDS mg/l	0.31 NS	0.32 NS	0.38 *	0.40 *	0.46 *	0.39 *	0.33 NS
Summer (14 July, 2017)							
CHL-a mg/l	0.03 NS	0.03 NS	0.11 NS	0.22 NS	0.33 NS	0.07 NS	0.06 NS
DOM mg/l	-0.002 NS	0.01 NS	0.08 NS	0.21 NS	0.23 NS	0.02 NS	0.01 NS
Turbidity NTU	0.05 NS	0.07 NS	0.12 NS	0.23 NS	0.22 NS	0.01 NS	0.01 NS
TSS mg/l	0.01 NS	0.05 NS	0.16 NS	0.24 NS	0.27 NS	0.08 NS	0.06 NS
TDS mg/l	-0.12 NS	-0.07 NS	0.05 NS	0.08 NS	0.12 NS	0.01 NS	-0.01 NS
Autumn (18 October, 2017)							
CHL-a mg/l	0.23 NS	0.19 NS	0.40 *	0.32 NS	0.22 NS	0.08 NS	0.06 NS
DOM mg/l	0.30 NS	0.28 NS	0.44 *	0.40 *	0.19 NS	0.07 NS	0.06 NS
Turbidity NTU	0.32 NS	0.31 NS	0.47 *	0.35 *	0.10 NS	-0.01 NS	-0.02 NS
TSS mg/l	0.15 NS	0.17 NS	0.36 *	0.21 NS	0.03 NS	-0.09 NS	-0.09 NS
TDS mg/l	0.22 NS	0.21 NS	0.35 *	0.23 NS	0.05 NS	-0.06 NS	-0.07 NS

Significant correlation at P <0.01, Significant correlation at P <0.05, NS= Non-significant correlation.

Table 5: Accepted regression models of water quality parameters of Al-Gharraf River stations on the reflectance values at Bands 1, ...,7

Water quality parameter	**Regression model***	R^2
Chlorophyll-a (CHL-a)	CHL-a= 0.102 + 0.0073Band4	0.109
	CHL-a= 0.065 + 0.011Band5	0.099
	CHL-a= 0.112 + 0.0045Band3	0.091
	CHL-a= 0.067 + 0.0038Band1	0.075
	CHL-a= 0.072 + 0.0037Band2	0.069
Dissolving Organic Matter (MOD)	DOM= 0.073 + 0.0034Band5	0.094
	DOM= 0.101 + 0.0034Band4	0.021
	DOM= 0.115 + 0.0014Band3	0.0079
Turbidity (NTU)	NTU= 0.105 – 0.00046Band2	0.165
	NTU= 0.144 – 0.00041Band3	0.115
	NTU= 0.149 – 0.00056Band4	0.101
	NTU= 0.137 – 0.00087Band5	0.094
Total Suspended Solid (TSS)	TSS= 0.125 – 0.00060Band2	0.306
	TSS= 0.163 – 0.00056Band3	0.243
	TSS= 0.177 – 0.00079Band4	0.222
	TSS= 0.157 – 0.00110Band7	0.221
	TSS= 0.176 – 0.00116Band5	0.185
Total Dissolved Solid (TDS)	TDS= 0.131 – 0.000066Band6	0.221
	TDS= 0.164 – 0.000055Band4	0.182
	TDS= 0.108 – 0.000034Band2	0.165
	TDS= 0.151 – 0.000035Band3	0.164
	TDS= 0.155 – 0.000078Band5	0.144

* Selected models have the highest R^2

Chlorophyll-a (CHL-a).

Chlorophyll-a is green pigment found in all photosynthetic organisms such as plants, algae, and cyanobacteria. CHL-a is key indicator of the eutrophication because it acts as a link between nutrient concentration (nitrogen and phosphorus) and algal growth. Moreover, it is one of the photosynthetic agents, contributing to the colour of the water (Liu, *et al.*, 2010).

In this study remote sensing results demonstrated that band 2 is highly significantly correlated with CHL-a in winter (January), with a highest R^2 value of 0.069, as given in Table (4 and 5). Whereas, band 3 (green region) most likely significantly correlated with CHL-a in spring (April), and autumn (October) with a highest R^2 value of 0.091. However, band 5 (NIR region) highly significantly correlated with CHL-a in spring (April), with highest R^2 value of 0.099.

Gitelson *et al.*, (2008), refer that CHL-a mainly reflecting at the spectral wavelength around 550 nm (green region) and 700 nm (NIR boundary region) as a result of strong absorption by CHL-a at the wavelength of approximately 450-475 nm in the blue region and at near 670 nm in the red region. The reflectance peak near 700 nm and its ratio to the reflectance at 670 nm could be used to accurately measure the CHL-a concentration in turbid waters.

Han and Jordan (2005), carry out study on the behavior of the reflectance peak near 700 nm and concluded that the 700 nm reflectance peak was important for the remote sensing of inland and coastal waters, especially for measuring chlorophyll concentration. Furthermore, most researchers have concluded that increasing CHL-a concentration causes a decrease in the spectral response at short wavelengths, especially in the blue band as shown in Figure (5).

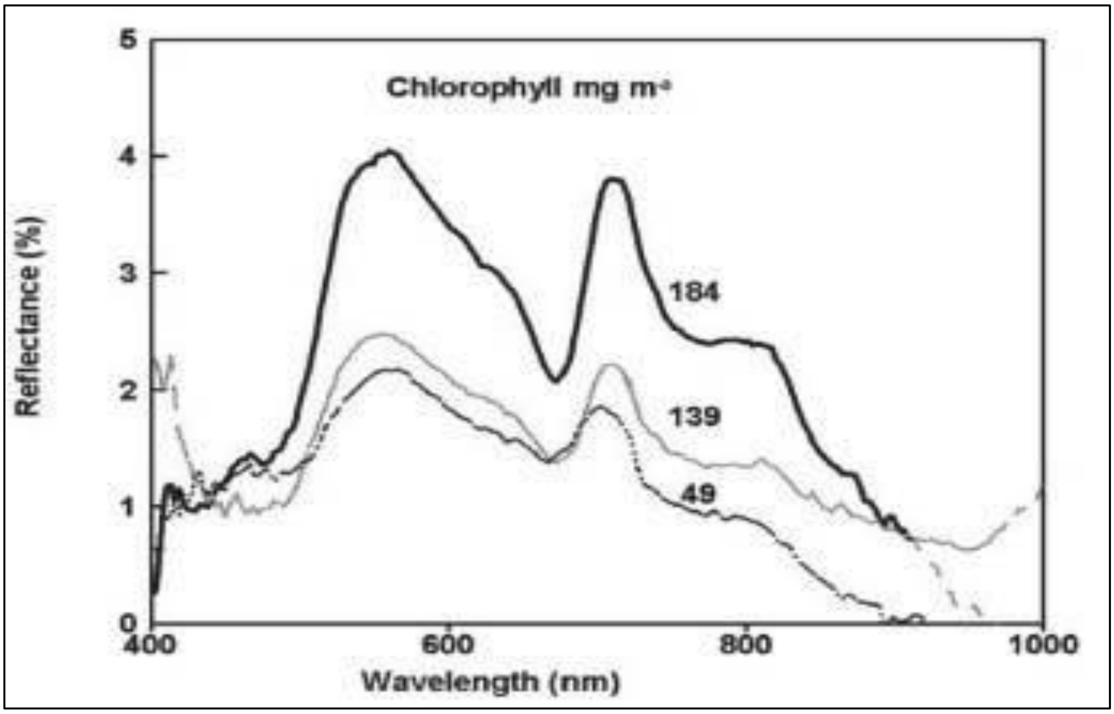

Fig. 5: The relationship between reflectance and wavelength as affected by the concentration of chlorophyll-a

One ther side, the seasonal changes of the Landsat 8 OLI imageries provides that CHL-a concentrations are higher value at Midle Al-Shatrah station in spring (March to April), Summer (August) and autumn (October to November), whereas lower value at the Entrance Kut station in most of months as displayed in Figure (6). The highest CHL-a values in April and October would be related to phytoplankton blooms, this indicates the high of eutrophication phenomenon in the Al-Gharraf River during the investigated period. This work findings are coincided with other results of backed by Alparslan *et al.*, (2007), Ahmed and Al-Khafaji (2013), Blondeau, *et al.*, (2014), and Kim *et al.*, (2017).

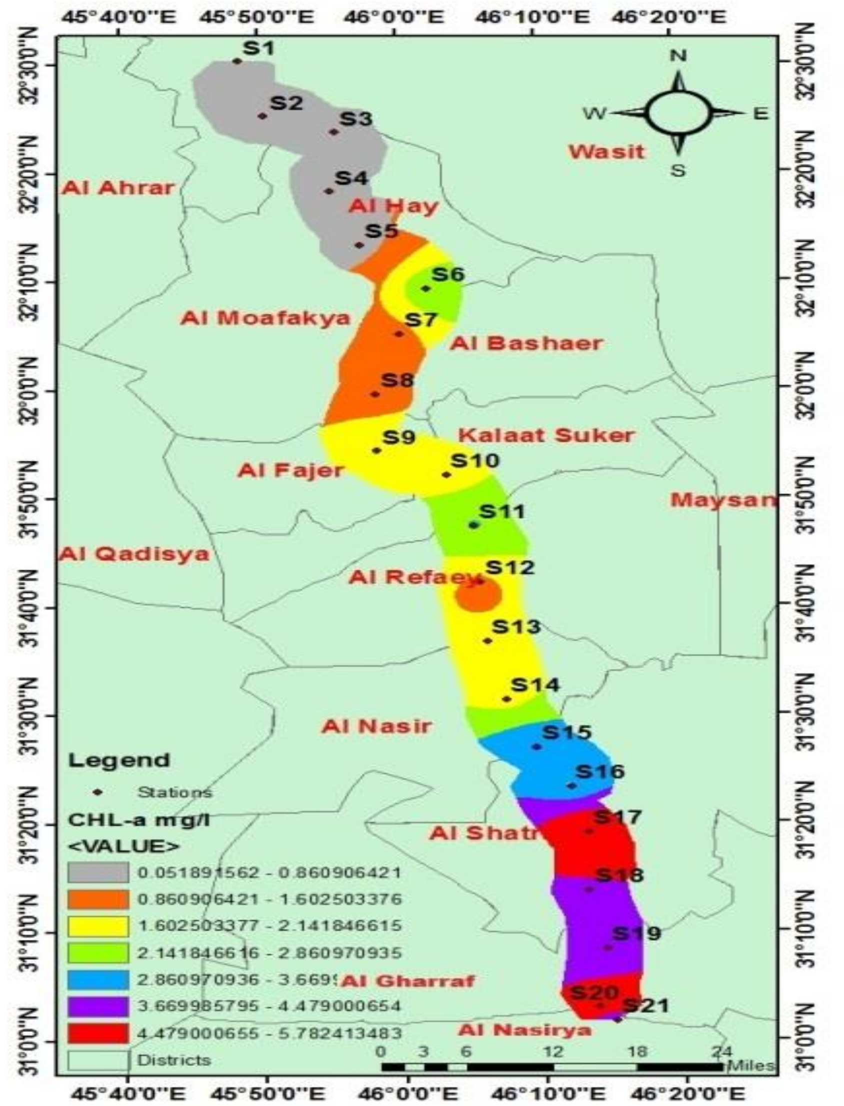

Fig. 6: Map of chlorophyll-a map

Dissolved Organic Matter (DOM).

The terms of the DOM reffer to all soluble organic matter those contribute significantly to the absorption light at certain wavelengths, also called colored dissolved organic matter (CDOM), aquatic humus, and gelbstoff or yellow matter, consists of naturally occurring, water-soluble, biogenic, heterogeneous organic substances that are yellow to brown in color, which exist in both fresh and saline waters. These compounds are brown and can color the water yellowish brown in high concentrations (Abu Daya, 2004).

The statistical analysis indicate that the band 3 (green region) is highly significantly correlated with DOM in winter (January) and autumn (October) with a highest R^2 value of 0.0079, as presented in Table (4 and 5). On other hand, band 2 (blue region), and band 4 (red region) significantly correlated with DOM in spring (April), with a highest R^2 value of 0.021. Band 5 (NIR) significantly correlated with DOM in spring (April), with highest R^2 value of 0.094. And band 3 significantly correlated with DOM in autumn (October).

Bukata *et al.,* (1995), mention that DOM does not significantly affect the scattering within the water colum, DOM absorbs light in both ultraviolet and visible range and affects the volume reflectance spectrum but almost exclusively at the shorter wavelengths.

Miller *et al.,* (2002), indicate that the increase in the DOM concentration mainly affects the reflectance values in the blue and green region of the spectrum (especially below 500 nm) and its absorbance increases exponentially with decreasing wavelength. This effect can complicate the use of CHL-a retrieval algorithms and phytoplankton production models that are based on remotely sensed ocean color.

The Landsat 8 OLI derived DOM images show that DOM is lower value in the stations of the Wasite Governorate except Mid Al-Hayy station during winter (February) and spring (March and May). While DOM is higher value in the stations of the Dhi-Qar Governorate, during summer (June and July) and autumn (November) as presented in Figure (7). The highest content of DOM were in warm season that might be because of the rise of temperature and increasing active of microorganisms which decomposes the dead parts from plants and animals, whereas the lowest content were in the cool season when the temperature is low and the active of decomposers is declined (Bass and Potts, 2001).

Ritchie *et al.*, (2003), and Mannino *et al.*, (2008), point out that remote sensing of DOM is important in studying aquatic environment and carbon dynamics, therefore, data of remote sensing provides an efficient method to estimate DOM concentration within a large spatial and temporal scale.

Moreover, no studies has been done on remote sensing technique related to Al-Gharraf River, but this the study supported by several researchers which used remote sensing technique for assessing the water quality like studies of Shen *et al.*, (1998), on Changjiang River in USA, Maillard and Pinheiro (2008), on Velhas River in Brazil, and El-Zeiny and El-Kafrawy (2017) on Burullus Lake in Egypt.

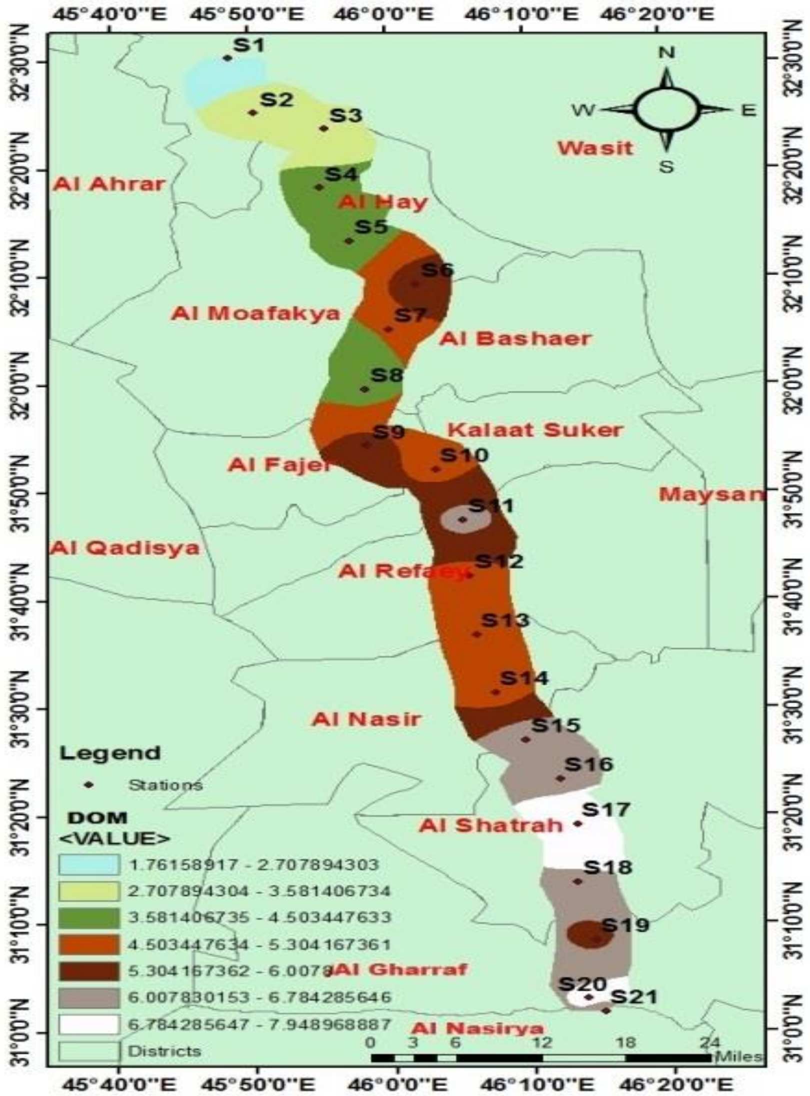

Fig. 7: Map of Dissolved Organic Matter

Turbidity (NTU)

Turbidity defined as an expression of the optical property of a medium which causes light to be scattered and absorbed rather than transmitted in straight lines through the sample and it is an important water quality variable (Lawler *et al.*, 2006).

The obtained results showed that band 5 (NIR region) is highly significantly correlated with turbidity in spring (April), with a highest R^2 value of 0.094, as shown in Table (4 and 5). while, band 3 (green region) most likely significantly correlated with turbidity in autumn (October), with a highest R^2 value of 0.115. Band 4 (red region) significantly correlated with CHL-a autumn (October), with highest R^2 value of 0.101.

Figure (8), describe seasonal variation of the Landsat 8 OLI imageries provides that turbidity (NTU) concentrations are higher value at Midle Al-Shatrah station in winter (February), and autumn (October to November), whereas lower value at the Entrance Kut station in most of months. The highest turbidity values in February, October, and November would be related to soil erosion in the nearby catchment and massive contribution of suspended solids from watewater. Surface runoffs and domestic wastes mainly contribute to the increased turbidity (Gangwara *et al.*, 2012).

Many researcher refer that an increase of turbidity in waterbodies causes the peak of visible reflectance to shift from the green region (clearer water) toward the red region of the spectrum. Also found that the first four bands of Landsat are well correlated with total suspended matter (Brezonik *et al.*, 2005 and Akbar, 2010).

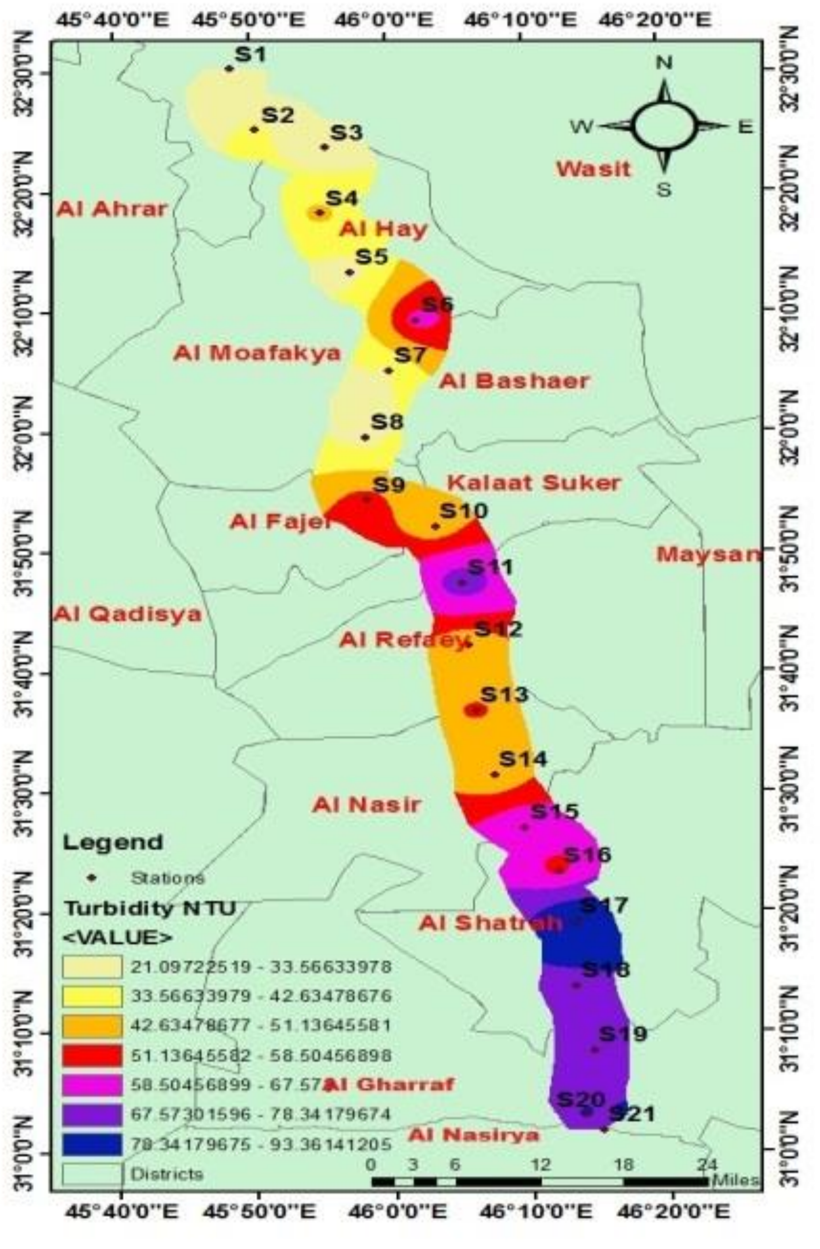

Fig. 8: Map of turbidity

Total Suspended Soiled (TSS)

Total Suspended Solid remaining on the filter paper after filtration which including clay, silt, sand, mineral particles; phytoplankton, heterotrophic plankton, and particulate organic detritus. It absorbs heat from sunlight and increases water temperature. Therefore, phytoplankton and the heterotrophic community it supports contribute to what is measured by TSS. In particular, a reduction in chlorophyll-a will be accompanied by a proportional reduction in TSS due to the dry weight component of phytoplankton (Myint and Walker, 2002)

Current statisticall analysis results revealed that band 3 (green region) and band 4 (red region) is highly significantly correlated with TSS in winter (January), with a highest R^2 value of 0.243, as presented in Table (4 and 5). On other hand band 5 (NIR region) most likely significantly correlated with TSS in spring (April), with a highest R^2 value of 0.185.

Lim and Choi (2015), by in situ studies showed that suspended solids was correlated with Bands 2–5 of Landsat 8 OLI, and constructed 3 multiple regression models through single bands of OLI. However, most researchers have concluded that surface suspended sediments can be mapped and monitored in large water bodies using sensors available on current satellites.

Ritchie *et al.* (1990), using in situ studies,refer that suspended sediments increase the radiance emergent from surface waters in the NIR proportion of the electromagnetic spectrum. As well as, concluded that wavelengths between 700 and 800 nm were most useful for determining suspended sediments in surface water, as shown in Figure (9).

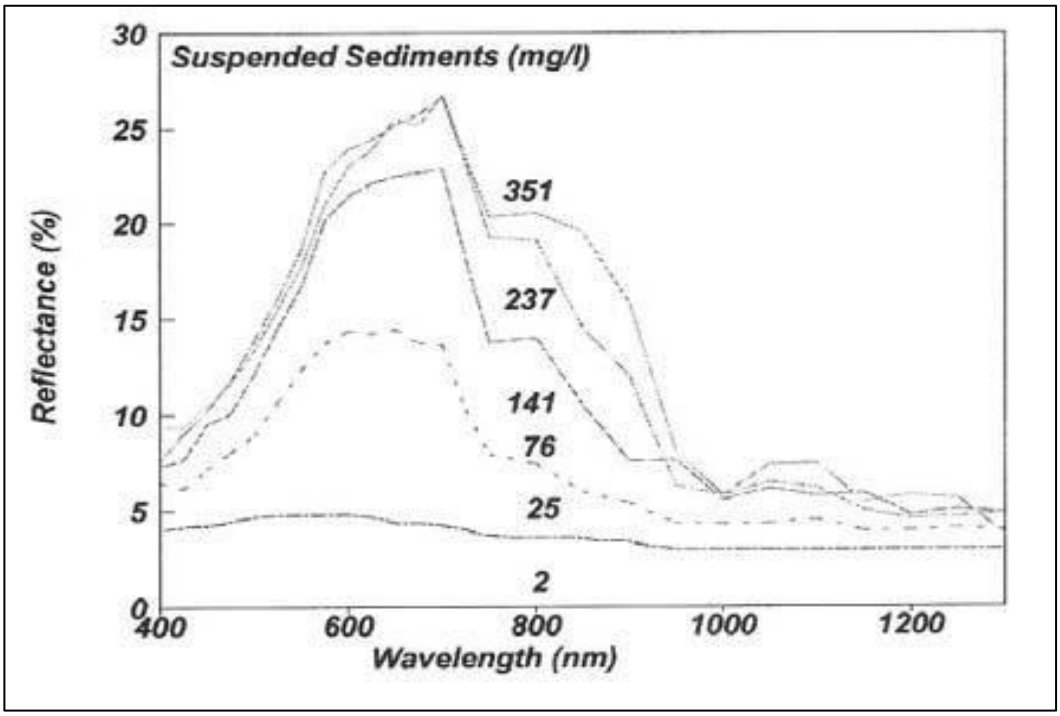

Fig. 9: The relationship between reflectance and wavelength as affected by the concentration of suspended sediments

On other side, general spatial distributions of the Landsat 8 OLI imageries derived seasonally TSS reveal that maximum value of TSS along the Al-Gharraf River (especially, Mid Al-Hayy, End Qalat Suker, End Naser, Mid Al-Shatrah and Mid Al-Gharraf stations) and minimum value in other stations of Al-Gharraf River, as depicted in Figure (10). The TSS values are highest in autumn (November) and lowest in summer months (June to August) in all sites.

These results didn't correspond with those of Richards (1999), Doxaran *et al.,* (2002), Martinez *et al.,* (2007), Nechad *et al.,* (2010), Lee *et al.,* (2013) and Thakur *et al.,* (2017).

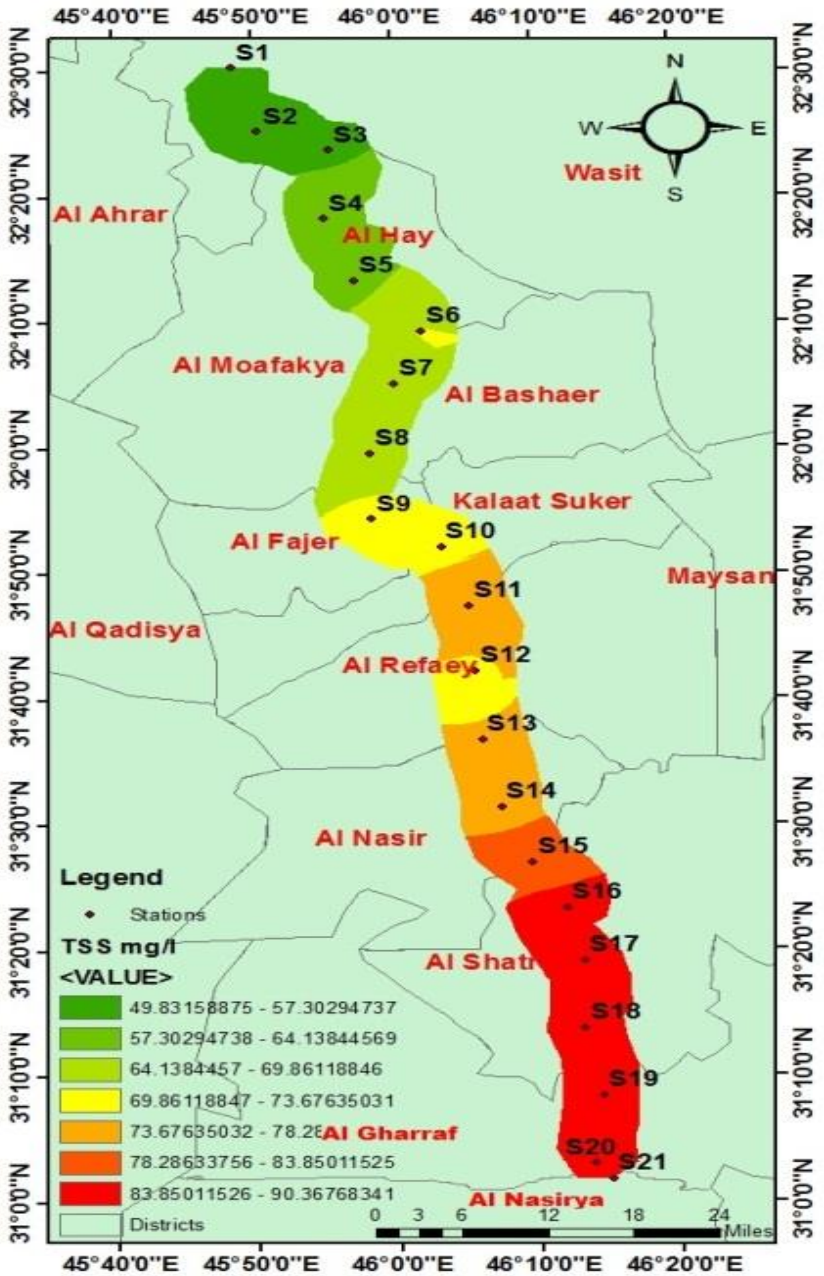

Fig. 10: Map of total suspended solid

Total Dissolved Soiled (TDS)

TDS is the term used to describe the inorganic salts and small amounts of organic matter present in solution in water. The concentration of TDS in natural waters are determined by the geology of the discharge, atmospheric precipitation and the water balance (Zipper and Berenzweig, 2007).

Present study findings showed that band 5 (NIR region) is most highly significantly correlated with TDS in spring (April), with a highest R^2 value of 0.144, as indicate in Table (4 and 5). Whereas, band 3 (green region) likely significantly correlated with TDS in autumn (October), with a highest R^2 value of 0.164.

Data of the Landsat 8 OLI derived TDS images demonstrated that TDS is lower value in the first eight stations of the Al-Gharraf River (from Entrance Kut to Entrance Fajer), except Mid Al-Hayy station during summer (June to August). While TDS is higher value in last ten stations of the Dhi-Qar Governorate, during winter (December to February) and autumn (Sptember to November) as shown as Figure (11).

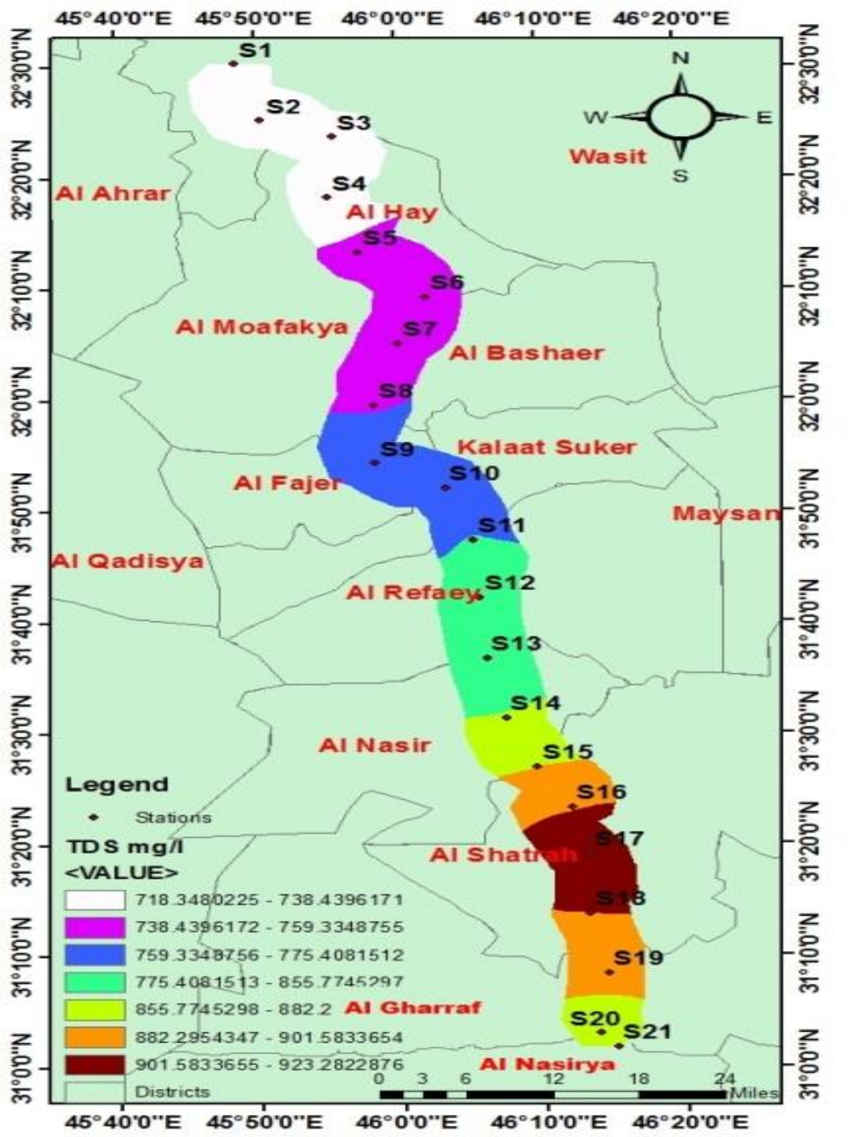

Fig. 11: Map of total dissolved solid

CONCLUSION

The current study has proven the remotely sensed image and GIS tool can be used to maps the spatial distribution of CHL-a, DOM and TSS, with sufficient accuracy for reflectance of Landsat 8 OLI bands at twenty-one stations along the Al-Gharraf River. We suggested to analyze the relationship between water quality parameters and other high resolution satellites images such as IKONOS, MODIS, and SPOT then compare them with the results that was taken from LANDSAT 8 OLI image.

Acknowledgments

The authors wish to express their gratitude to the Iraqi Ministry of Health and Environment /Center of Ecological Researches for providing support to carry out this work.

REFERENCES

1. Abdullah, H. (2013). Water Quality Assesnent of Dokan Lak using Resolu High Spatial Resolution of Lsndsat 8OLI. Msc. Thesis. *College of Civil Engineering, University of Sailimania, Iraq*.
2. Daya, M. A. (2004, February). Coastal water quality monitoring with remote sensing in East Kalimantan, Makassar strait, Indonesia. ITC.
3. Ahmed, M., & Al-Khafaji, A. (2013). Assessment Environmental Changes in Al-Habbaniya Lake and Surrounding Areasin the Central Part of Iraq. *Assessment*, *3*(4).
4. Akbar, T., Hassan, Q., & Achari, G. (2010). A remote sensing based framework for predicting water quality of different source waters. *The International Archives of Photogrammetry, Remote Sensing and Spatial Information Sciences*, *34*, 1-4.

5. Alparslan, E., Aydöner, C., Tufekci, V., & Tüfekci, H. (2007). Water quality assessment at Ömerli Dam using remote sensing techniques. *Environmental monitoring and assessment*, *135*(1), 391-398.
6. American Public Health Association. (1926). *Standard methods for the examination of water and wastewater* (Vol. 6). American Public Health Association.
7. Bass, D. (2001). Invertebrate community Composition and Physiochemical Conditions of Boehler Lake. In *Proceedings of the Oklahoma Academy of Science* (pp. 21-29).
8. Blondeau-Patissier, D., Gower, J. F., Dekker, A. G., Phinn, S. R., & Brando, V. E. (2014). A review of ocean color remote sensing methods and statistical techniques for the detection, mapping and analysis of phytoplankton blooms in coastal and open oceans. *Progress in oceanography*, *123*, 123-144.
9. Brezonik, P., Menken, K. D., & Bauer, M. (2005). Landsat-based remote sensing of lake water quality characteristics, including chlorophyll and colored dissolved organic matter (CDOM). *Lake and Reservoir Management*, *21*(4), 373-382.
10. Bukata, R. P., Jerome, J. H., Kondratyev, A. S., & Pozdnyakov, D. V. (2018). *Optical properties and remote sensing of inland and coastal waters*. CRC press.
11. Doxaran, D., Cherukuru, N., & Lavender, S. J. (2006). Apparent and inherent optical properties of turbid estuarine waters: measurements, empirical quantification relationships, and modeling. *Applied optics*, *45*(10), 2310-2324.
12. El-Zeiny, A., & El-Kafrawy, S. (2017). Assessment of water pollution induced by human activities in Burullus Lake using Landsat 8 operational land imager and GIS. *The Egyptian journal of remote sensing and space science*, *20*, S49-S56.
13. Fan, C. (2014). Spectral analysis of water reflectance for hyperspectral remote sensing of water quailty in estuarine water. *Journal of Geoscience and Environment Protection*, *2*(02), 19.
14. Singh, J., Gangwara, R. K., Khare, P., & Singh, A. P. (2012). Assessment of physico-chemical properties of water: River Ramganga at Bareilly. *Journal of Chemical and Pharmaceutical Research*, *4*, 4231-4234.
15. Brezonik, P., Menken, K. D., & Bauer, M. (2005). Landsat-based remote sensing of lake water quality characteristics, including chlorophyll and colored dissolved organic matter (CDOM). *Lake and Reservoir Management*, *21*(4), 373-382.
16. Gholizadeh, M. H., Melesse, A. M., & Reddi, L. (2016). A comprehensive review on water quality parameters estimation using remote sensing techniques. *Sensors*, *16*(8), 1298.
17. Gitelson, A. A., Dall'Olmo, G., Moses, W., Rundquist, D. C., Barrow, T., Fisher, T. R., ... & Holz, J. (2008). A simple semi-analytical model for remote estimation of chlorophyll-a in turbid waters: Validation. *Remote Sensing of Environment*, *112*(9), 3582-3593.
18. Han, L., & Jordan, K. J. (2005). Estimating and mapping chlorophyll-a concentration in Pensacola Bay, Florida using Landsat ETM+ data. *International Journal of Remote Sensing*, *26*(23), 5245-5254.
19. Kim, H. C., Son, S., Kim, Y. H., Khim, J. S., Nam, J., Chang, W. K., ... & Ryu, J. (2017). Remote sensing and water quality indicators in the Korean West coast: Spatio-temporal structures of MODIS-derived chlorophyll-a and total suspended solids. *Marine Pollution Bulletin*, *121*(1-2), 425-434.
20. Lawler, D. M., Petts, G. E., Foster, I. D., & Harper, S. (2006). Turbidity dynamics during spring storm events in an urban headwater river system: The Upper Tame, West Midlands, UK. *Science of the Total Environment*, *360*(1-3), 109-126.
21. Lee, H. J., Park, J. Y., Lee, S. H., Lee, J. M., & Kim, T. K. (2013). Suspended sediment transport in a rock-bound, macrotidal estuary: Han Estuary, Eastern Yellow Sea. *Journal of Coastal Research*, *29*(2), 358-371.
22. Lim, J., & Choi, M. (2015). Assessment of water quality based on Landsat 8 operational land imager associated with human activities in Korea. *Environmental monitoring and assessment*, *187*, 1-17.
23. Niu, L., Luo, X., Hu, S., Liu, F., Cai, H., Ren, L., ... & Yang, Q. (2020). Impact of anthropogenic forcing on the environmental controls of phytoplankton dynamics between 1974 and 2017 in the Pearl River estuary, China. *Ecological Indicators*, *116*, 106484.
24. Ji LuYan, J. L., Geng XiuRui, G. X., Sun Kang, S. K., Zhao YongChao, Z. Y., & Gong Peng, G. P. (2015). Target detection method for water mapping using Landsat 8 OLI/TIRS imagery.
25. Maillard, P., & Santos, N. A. P. (2008). A spatial-statistical approach for modeling the effect of non-point source pollution on different water quality parameters in the Velhas river watershed–Brazil. *Journal of Environmental Management*, *86*(1), 158-170.
26. Mannino, A., Russ, M. E., & Hooker, S. B. (2008). Algorithm development and validation for satellite-derived distributions of DOC and CDOM in the US Middle Atlantic Bight. *Journal of Geophysical Research: Oceans*, *113*(C7).
27. Martinez, J. M., Guyot, J. L., Cochonneau, G., & Seyler, F. (2007, July). Surface water quality monitoring in large rivers with MODIS data application to the amazon basin. In *2007 IEEE International Geoscience and Remote Sensing Symposium* (pp. 4566-4569). IEEE.
28. Miller, R. L., DelCastillo, C. E., Powell, R. T., DSa, E., & Spiering, B. (2002). *Mapping CDOM Concentration in Waters Influenced by the Mississippi River Plume* (No. NASA/SE-2002-04-00035-SSC).
29. MOA& and I,1991. Ministry of Agriculture and Irrigation Republic of Iraq, State Commission for Irrigation and Reclamation Projects, Al-Furat Center for Studies and Designs of Irrigation

Projects, East Gharraf Project AL-Hai South Zone, Sector (A) , irrigation & drainage system of the main canal and drainage pumping station, July 1991.
30. Myint, S. W., & Walker, N. D. (2002). Quantification of surface suspended sediments along a river dominated coast with NOAA AVHRR and SeaWiFS measurements: Louisiana, USA. *International Journal of Remote Sensing*, *23*(16), 3229-3249.
31. Nechad, B., Ruddick, K. G., & Park, Y. (2010). Calibration and validation of a generic multisensor algorithm for mapping of total suspended matter in turbid waters. *Remote Sensing of Environment*, *114*(4), 854-866.
32. Ritchie, J. C., Zimba, P. V., & Everitt, J. H. (2003). Remote sensing techniques to assess water quality. *Photogrammetric engineering & remote sensing*, *69*(6), 695-704.
33. Ritchie, J. C., Cooper, C. M., & Schiebe, F. R. (1990). The relationship of MSS and TM digital data with suspended sediments, chlorophyll, and temperature in Moon Lake, Mississippi. *Remote Sensing of environment*, *33*(2), 137-148.
34. Schmugge, T. J., Kustas, W. P., Ritchie, J. C., Jackson, T. J., & Rango, A. (2002). Remote sensing in hydrology. *Advances in water resources*, *25*(8-12), 1367-1385.
35. Huanting, S. (1998). Change of the discharge and sediment flux to estuary I Changjiang River. *Health of the Yellow Sea*, 129-148.
36. Thakur, J.K.; Singh, S.K. & Ekanthalu, V. Sh. (2017). Integrating remote sensing, geographic information systems and global positioning system techniques with hydrological modeling. *Appl Water Sci* Vol.7:1595–1608.
37. USGS (United States Geological Survey), 2015. Landsat—A Global Land-Imaging Mission. [Online] Available at: http://remotesensing.usgs.gov.
38. Zipper, C. E., & Berenzweig, J. (2007). Total dissolved solids in Virginia freshwater streams: an exploratory analysis. *A Report to Virginia Department of Environmental Quality*.